

Flood inundation mapping using Sentinel-1A in An Giang province in 2019

Thi Hong Diep Nguyen^{1*}, Trong Can Nguyen², Thi Ngoc Tran Nguyen³, Thien Nhi Doan³

¹College of Environment and Natural Resources, Can Tho University, Vietnam

²King Mongkut's University, Thailand

³Can Tho University, Vietnam

Received 24 August 2020; accepted 20 November 2020

Abstract:

An Giang is one of the provinces in the Mekong delta that is greatly affected by flood events, which brings damage and devastation to life and property. This study practices the application of Sentinel-1A images to monitor the distribution of flood depths in the An Giang province in 2019 as well as applies regression correlation and thresholding to scattering value analysis. The research results indicated the exponential regression model on the VV polarization images had correlation coefficients (r) in August, September, and October ranging from 0.8398 to 0.9764 and determination coefficients (R^2) ranging from 0.7896 to 0.9533. Results from the map of current flood depth showed that the flood depth ranged from 0-250 cm, which corresponded to four flood levels. The flood area increased from August to October with the largest flooded area being 89,606.82 ha (accounting for 26.15%) mainly on rice lands and in eight urban districts including An Phu, Tinh Bien, Chau Thanh, Chau Phu, Phu Tan, Tri Ton, Chau Doc, and Long Xuyen city. The limit of flood depth determined by using the Sentinel-1A images was below 145 cm. Above this value, the scattering in the image is not significantly different from the actual submerged depth.

Keywords: An Giang province, backscatter, correlation regression, flood depth, Sentinel-1A.

Classification number: 5.1

Introduction

The Mekong delta is located in the low-lying area of the Mekong river basin and has an important role in Vietnamese economy. The Mekong delta is vulnerable to climate change and flood-related disasters. Recently, the Vietnamese part has been severely impacted by an increased frequency of floods and unusually large flooded areas more than any other country in the Mekong river basin. Each year, about half of the delta is flooded by overflow 1 to 3 meters in depth. This area's vulnerability to flooding thus creates a large negative impact on economic development not only in the region, but also in Vietnam as a whole. An Giang is the upstream province of the Mekong river delta thus the water depth and flood duration is higher and longer than in other provinces in the region. Families living in the low-level region of the inland areas in the Mekong river delta, especially in the An Giang province, has suffered the most from the annual flooding [1].

It is necessary to detect flood water levels to determine the magnitude of inundation, water level magnitude, and their variations, which are utilized to monitor the flooding extent. Remote sensing is one of the most promising applications to estimate flood level via satellite altimetry data. Satellite altimetry data includes the ERS-2, ENVISAT, and TOPEX/Poseidon satellites that are used to monitor water levels in rivers, lakes, and floodplains [2-5]. However, the flood water level of the entire flood areas is impossible to examine using this method because satellite altimeters only measure the water level of places due to their orbits. Therefore, another approach applied to calculate flood water levels combines flood area estimation and DEM. According to [6], flood water depths were classified from satellite images and labelled as shallow, medium, and deep using digital elevation data. Combined with these flood depths and physiographic and geological data, flood hazard maps were created. The authors [7, 8] combined DEMs and high-resolution images to measure the water levels of rivers and produced flood inundation maps. The authors [9, 10] performed flood water level calculations using satellite images and identified a simple linear regression to calculate flood depths by a given flood event. Apart from initial studies, several research works have concentrated on improving estimation accuracy [11-14]. Review articles [15, 16] are also available. Since the mid

*Corresponding author: Email: nthdiep@ctu.edu.vn

1990s, with the advantages of synthetic aperture radar (SAR), satellite images have become available and developed for flood monitoring [17], which has continued to improve with launches of very high-resolution SAR satellites over the past decade, particularly, TerraSAR-X by the German Aerospace Center (DLR), Radarsat-2 by the Canadian Space Agency (CSA), and also constellations of COSMO-SkyMed, by the Italian Space Agency (ASI), and Sentinel-1, by the European Space Agency (ESA). Synthetic aperture radar data has the advantage of the ability to create flood mapping through cloud cover and can remain largely unimpacted by adverse weather conditions that often exist during high-impact flood events [18]. This innovation has brought higher reliability to flood mapping and has accelerated flood forecasting progress and flood inundation model development particularly in calibration and validation modelling of the area [19-27] and more recently assimilation [8].

This study aims to develop an estimation method of flood water level for the measurement of water levels on floodplains surveyed through a combination of satellite images and adopted regression models to compute the flood depths of a given flood event. We selected the An Giang province as the study area, which is a flood-prone area with a complex system of canals and rivers. We applied SAR satellite images (i.e. Sentinel-1A data) for the developed method. The results using Sentinel-1A images were verified by comparison with ground observation data and floodplain points in the study area.

Study area and data

Study area (Fig. 1)

The Vietnam Mekong delta (VMD) is the end of the Mekong river. The An Giang province (10°12' N to 10°57' N and 104°46' E

to 105°35' E) is the first province of the VMD and it borders with Cambodia in the northwest (104 km long). An Giang's population is over 2.4 million (2019) [28] with a total area around 3,536 km² in which 70% of this area is used for agricultural production. There are two distinct seasons in this region that consists of dry and wet (monsoon). The wet season happens between May and November in which high rainfall usually appears in October and November at the end of the wet season. The flooding season occurs nearly at the same time as the rainfall season, leading to the risk of deep inundation. Because of the location's geography, there are two main branches of the Mekong river that flow through the province, namely, the Tien river and Hau river, which bring annual floods to the delta. Thus, An Giang annually faces flooding that is deeper and higher than other provinces. Since the strategy for intensive rice-cultivated production was developed by the Government of Vietnam [29], a full-dykes system that fully encloses the triple rice fields from flood water has been rapidly covering the An Giang province. Consequently, they affect the flood situation over the whole the province as well as in areas downstream [30].

Data used

The SAR sensor onboard the Sentinel satellite uses Terrain Observation with Progressive Scans SAR (TOP-SAR) to acquire images [31]. Level 1 Ground Range Detected (GRD) Sentinel 1A C-band scenes were collected for this study from the Copernicus Open Access Hub (<https://scihub.copernicus.eu>) on ESA's website. Level 1 GRD products concern SAR data detected, multi-looked, and projected to ground range using an earth Ellipsoid Model with an approximate square pixel resolution [32].

A total number of three GRD SAR scenes, in descending and ascending Interferometry Wide (IW) swath mode with polarization VV and VH, were collected spanning the period from August to

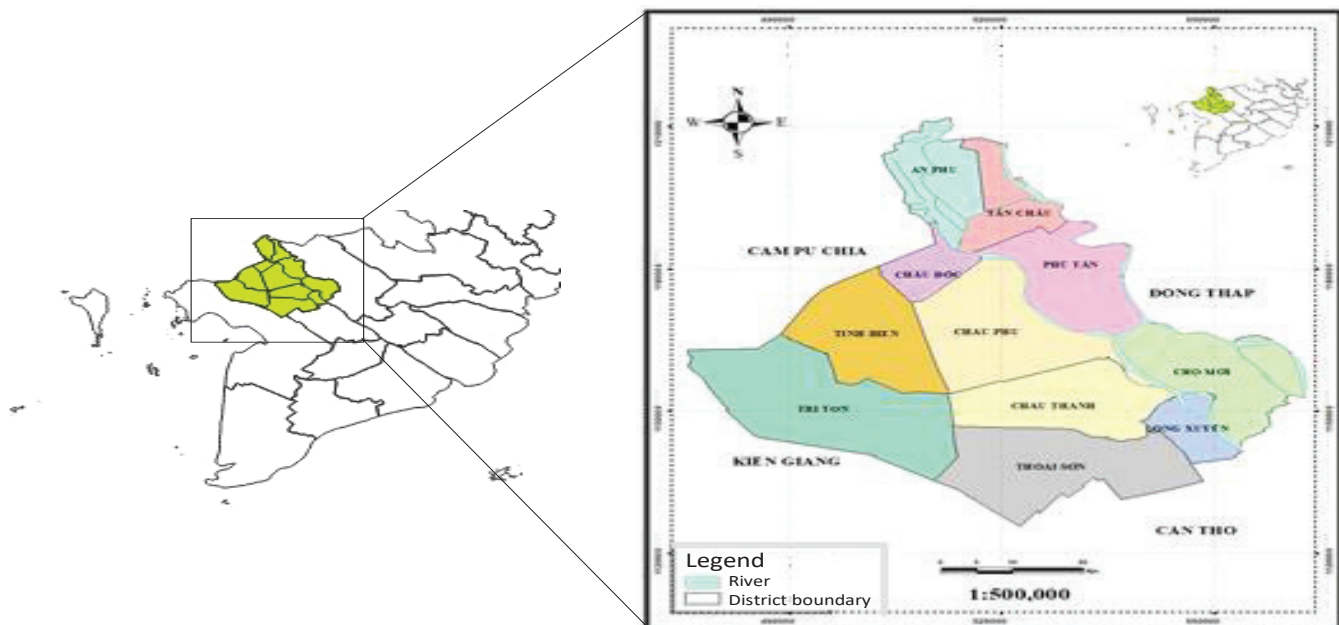


Fig. 1. Location of the study area.

October 2019 (Table 1). These data were processed and analysed to create binary water/non-water products as well as SAR multi-temporal products based on the contrast of the surface variations of land and water showing different back-scattering signatures.

Table 1. Catalogue of Sentinel-1 SAR scenes used.

No.	Scene Name	Date of capture	Resolution	Polarization
1	S1A_IW_GRDH_1SDV_20190806T111128_20190806T111153_028448_033705_9B94	06/08/2019	10 m	VV, VH
2	S1A_IW_GRDH_1SDV_20190911T111130_20190911T111155_028973_034937_F8F8	11/09/2019	10 m	VV, VH
3	S1A_IW_GRDH_1SDV_20191005T111131_20191005T111156_029323_035539_E66C	05/10/2019	10 m	VV, VH

Collection of water depth samples

Water depth samples were collected during the rainy season from August to October 2019, in flood cover in the An Giang province. Photographs were taken at each sample’s location, which had coordinates determined using the global positioning system (GPS) and the water depth measurement was made by a depth gauge. The sampling sites selection was conducted with a random sampling technique with 107 total samples with 15 samples in August, 40 samples in September, and 52 samples in October as shown in Fig. 2.

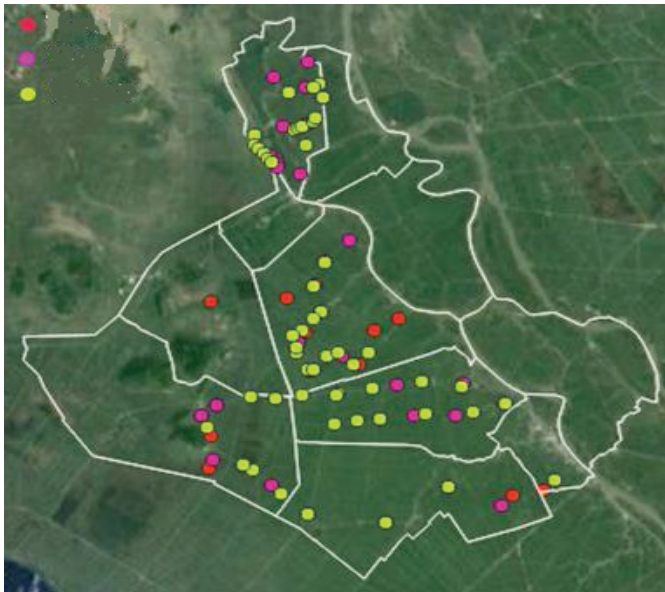


Fig. 2. Location of sampling sites.

Methodology

Data processing

The SAR Sentinel 1 images were processed with the free software SNAP (Sentinel Application Platform) Tool version 7.0.0. [33], which was created by ESA for data classification by Sentinel satellites. In addition, the spatial data validation processing steps are shown in Fig. 3. The image processing steps include: (1) delineating the targeted study area, a subset of the whole image

is created by setting the geographic coordinates values of study area; (2) adjusting image resolution, radiometric correction was processed to relate radar backscatter due to pixel values, thus, it is essential for quantitative image calibration to use the SAR data as pixel values to represent the reflecting surface of the true radar backscatter; (3) radiometric correction, this operation is necessary to produce multi-temporal products. With a calibration vector included, Sentinel-1 data allows the conversion of the image’s intensity values into sigma naught values (s_0). From this step onward, processing is generated for the two polarizations VH and VV that we provide [34, 35]; (4) geometric correction, a correction of geometric distortion caused by topography such as foreshortening and shadows using a digital elevation model correction to the location of each pixel; (5) image filtering, the main problem of SAR data is speckle “noise” caused by the random effect of many small individual reflectors within a given pixel. In order to reduce the speckle in SAR images, different adaptive filters were applied to preserve the radiometric and textural information and to enhance visualization at the same time. After comparison, the Lee filter uses mean and standard deviation with window size determination to assess different factors for smoothing (Fig. 3E). In homogeneous regions of flooded areas, the final pixel value is the linear average of neighbouring pixels [36]. Therefore, this filter uses a priori knowledge of the Probability Density Function (PDF) of the scene when suppressing the speckle of the scene [37, 38]; and (6) conversion of the image intensity values into a sigma naught value, which is a unitless backscatter coefficient that is converted to dB using a logarithmic transformation.

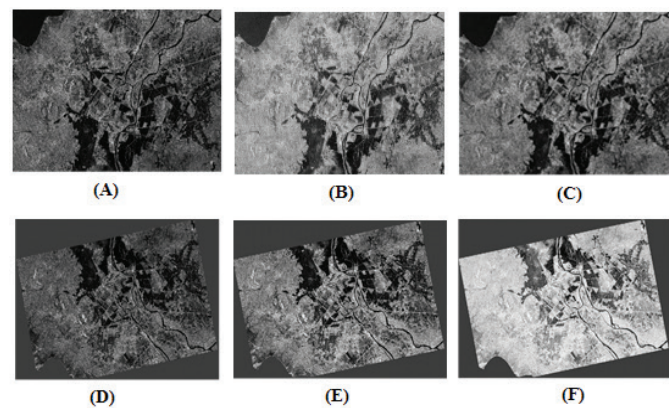


Fig. 3. (A) Delineating the target study area, (B) adjusting image resolution, (C) radiometric correction, (D) geometric correction, (E) image filtering, and (F) sigma naught values (dB).

The last common step in image pre-treatment is to perform a correction of the terrain and ortho-rectification. This mainly eliminates distortions due to changes in the topography and the angle of incidence with the ground with respect to the nadir. The geometric calibration used in this study was range Doppler terrain correction and the digital elevation model (DEM)–SRTM-3Sec to derive precise geolocation information. The map projection type of the output images was expressed in WGS84 geographic coordinates.

The above-mentioned actions are considered as pre-processing steps. In this study, two products were generated based on SAR data: i) binary images showing water and non-water areas over the study area and ii) multi-temporal SAR images combining two or three dates to show spatiotemporal occurrences and a seasonal evolution of the flood event.

For the water/non-water product generation, the image binarization technique was applied. The threshold segmentation algorithm, or histogram thresholding, is a simple, widely used, and effective method to generate a binary image [39]. The first step is to separate water from non-water areas through binarization and selection of a suitable threshold for each image. Low values of the backscatter corresponded to the water, while high values correspond to the non-water areas.

Regression model

Backscatter values at the measurement positions were extracted from the images with VV and VH polarities with the Point Sampling Tool on QGIS. Following the analysis of regression models in Excel, the appropriate form of the fit equation through the correlation between backscattering values on the image and the field depth of inundation was chosen.

Performance assessment

The flood depth performance was assessed and estimated using three statistical metrics parameters, namely, RMSE (Root Mean Square Error), MAE (Mean Absolute Error), and r (correlation coefficient).

$$RMSE = \sqrt{\frac{1}{n} \sum_{j=1}^n (x_i - X)^2} \tag{1}$$

$$r = \frac{\sum_{i=1}^n (x_i - \bar{x})(y_i - \bar{y})}{\sqrt{\sum_{i=1}^n (x_i - \bar{x})^2 \sum_{i=1}^n (y_i - \bar{y})^2}} \tag{2}$$

where x_i and y_i are the calculated and measured flood depth values the i^{th} sample, respectively; \bar{x} and \bar{y} are the mean values of the EC measurement and the flood depth values prediction, respectively; and n is the total number of samples used.

Results

Data collection

The correlation data and regression analysis/verification were completed from 107 flooding points in An Giang province as shown in Table 2.

Table 2. Data used for correlation and regression analysis.

No.	Date	Total measuring points	Total analysing points	Total regression points	Total inspection points	Excluded points
1	06/08/2019	15	12	07	05	03
2	11/09/2019	40	36	26	10	04
3	05/10/2019	52	48	33	15	04
Total		107	96	66	30	11

Regression models

Two regression models suitable for the study of flood depth including linear regression and exponential regression models were obtained from the results of the regression and correlation analysis (Table 3).

Table 3. The regression model equation used to estimate the flood depth of on each polarized Sentinel-1A image in 2019.

No.	Month	Polarization	Regression Model	r(η)	R ²
1	August	VV	DSN1=-0.9211*VV-1.7404	0.7545	0.5692
2			DSN2=1.6324*e ^{-0.143*VV}	0.7976	0.6361
3		VH	DSN3=-0.955*VH-8.3268	0.8204	0.673
4			DSN4=0.6974*e ^{-0.138*VH}	0.8055	0.6488
5	September	VV	DSN5=-3.9199*VV-28.351	0.8826	0.779
6			DSN6=0.4281*e ^{-0.247*VV}	0.7919	0.6271
7		VH	DSN7=-4.4258*VH-61.815	0.8218	0.6753
8			DSN8=0.0648*e ^{-0.267*VH}	0.7053	0.4975
9	November	VV	DSN9=-7.1994*VV-30.918	0.7119	0.5069
10			DSN10=1.8742*e ^{-0.21*VV}	0.8557	0.7322
11		VH	DSN11=-10.492*VH-144.03	0.7457	0.5561
12			DSN12=0.1152*e ^{-0.282*VH}	0.8275	0.6848

Table 3 shows that all 12 regression model equations have a negative correlation and the correlation and determination coefficients are greater than 0.5. The model with the highest coefficients is the linear regression model on the VV polarization in September with r and R² being 0.8826 and 0.779, respectively. In contrast, the model with the lowest r and R² coefficients is the linear regression model on the VV polarization in October with 0.7119 and 0.5069, respectively.

Validation flood depth models

The number of inspection points was 5 points in August, 10 points in September and 15 points in October. In the testing results of all regression models shown in Table 3, there was a correlation between the estimated flood depth in image and the field flood depth since the coefficient of determination R² is greater than 0.5. The most suitable regression model is the exponential regression model on the VV polarization with correlation coefficients, coefficients of determination, deviations (Bias), and root mean square errors (RMSE) given in Table 4 for August, September and October. The study used an exponential model to establish the maps of current flood depth status in each month in 2019.

Table 4. The relevance of the regression models through testing coefficients and the correlation between estimated flood depth and field flood depth in 2019.

No.	Month	Polarization	Inspected regression model	R	R ²	Bias (cm)	RMSE (cm)
1	August	VV	DSN1=-0.9211*VV-1.7404	0.6384	0.7999	-2.17	2.67
2		VV	DSN2=1.6324*e ^{0.143*VV}	0.8886	0.7896	-2.04	2.41
3		VH	DSN3=-0.955*VH-8.3268	0.8177	0.6687	-1.6	2.11
4		VH	DSN4=0.6974*e ^{0.138*VH}	0.8738	0.7636	-1.41	1.84
5	September	VV	DSN5=-3.9199*VV-28.351	0.9456	0.8941	6.78	11.99
6		VV	DSN6=0.4281*e ^{0.247*VV}	0.9764	0.9533	3.06	7.55
7		VH	DSN7=-4.4258*VH-61.815	0.8881	0.7887	2.56	14.06
8		VH	DSN8=0.0648*e ^{0.267*VH}	0.9555	0.9129	3.25	10.57
9	October	VV	DSN9=-7.1994*VV-30.918	0.8663	0.7505	-29.69	33.8
10		VV	DSN10=1.8742*e ^{0.21*VV}	0.8398	0.7052	2.29	17.93
11		VH	DSN11=-10.492*VH-144.03	0.5458	0.2979	-12.36	34.79
12		VH	DSN12=0.1152*e ^{0.282*VH}	0.6762	0.4573	-5.44	55.55

Flood depth mapping in 2019 in An Giang

Based on the selected regression model, flood depth maps were created in An Giang during three months from August to October in 2019. The maps contain flood depths that are graded according to a colour scheme from light to dark (Fig. 4). In August, the flooding level was low and it was concentrated on the four districts of Thoai Son, Chau Thanh, Chau Phu, and Phu Tan (Fig. 4A). By September, floods began to increase in both surface distribution and depth with a focus on areas without dikes in districts like An Phu, Tinh Bien, Chau Phu, Chau Thanh, Phu Tan, and Chau Doc city (Fig. 4B). Finally, in October, the flood surface continued to expand and the flood depth was at its highest this month. The flood area was distributed outside the dikes and expanded to eight districts including An Phu, Tinh Bien, Chau Thanh, Chau Phu, Phu Tan, Tri Ton, Chau Doc, and Long Xuyen city (Fig. 4C).

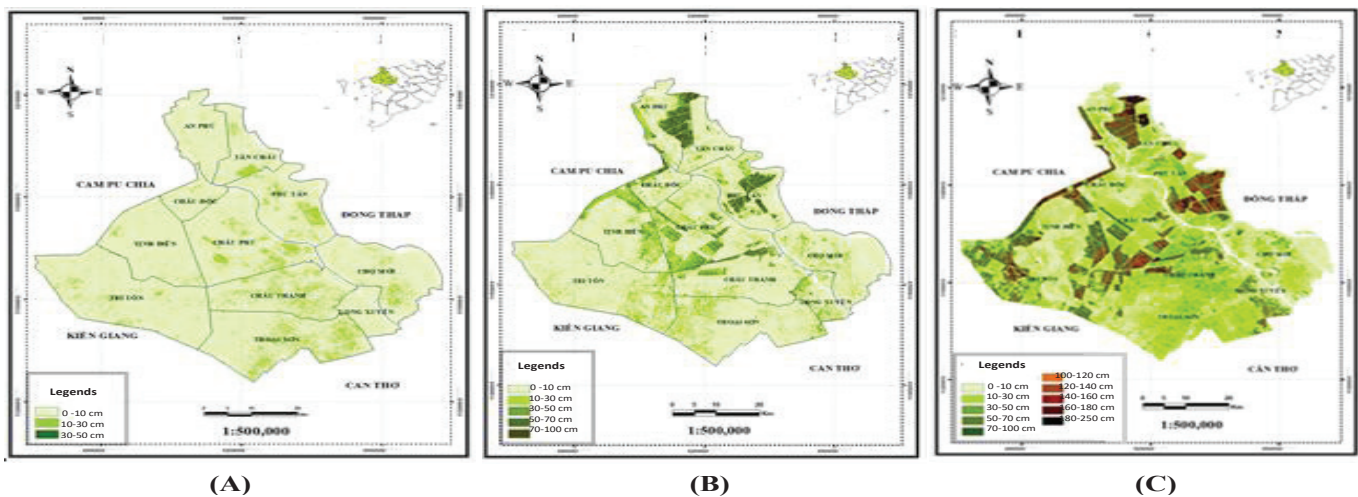


Fig. 4. The flood depth distribution in the An Giang province in 2019 (A) in August, (B) in September, and (C) in October.

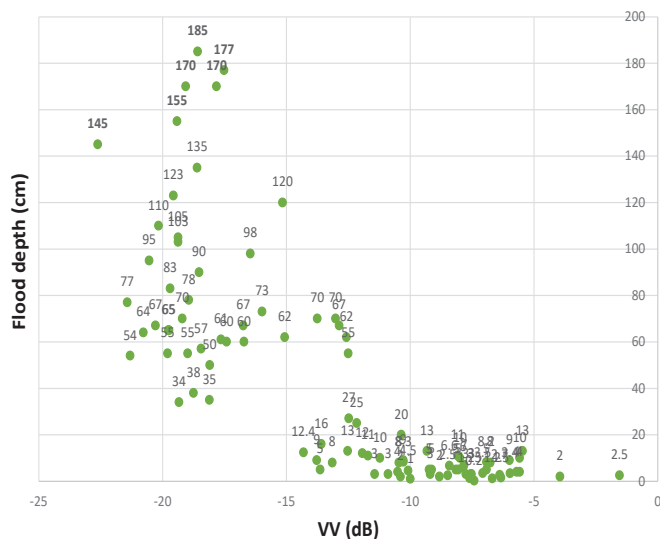


Fig. 5. Threshold diagram of field flood depth and backscattering values on VV polarization.

Estimation flood depth threshold on Sentinel-1A image

According to Fig. 5, the deeper the flood depth is, the lower the backscattering value on the VV polarization becomes and vice versa. However, when the depths range from 140-160 cm, there is a sudden change where the backscattering values decrease at a depth from above 145 cm to -22.6 dB. The data in Fig. 5 shows that the values of flood depth and backscattering are no longer in correlation over the depth of 145 cm, at which the backscattering values begin to go along the opposite direction (forward).

The flooding depths of more than 145 cm were tested to clarify that the thresholding results of the flood depth limit on Sentinel 1A images have eliminated depth value correlations to the backscattering values in each location where field depth values were measured. Fig. 6 shows the flood depth limit using the Sentinel-1A images below 145 cm, the depth values above 145 cm did not have a significant difference due to the backscattering value compared to the actual flood depth.

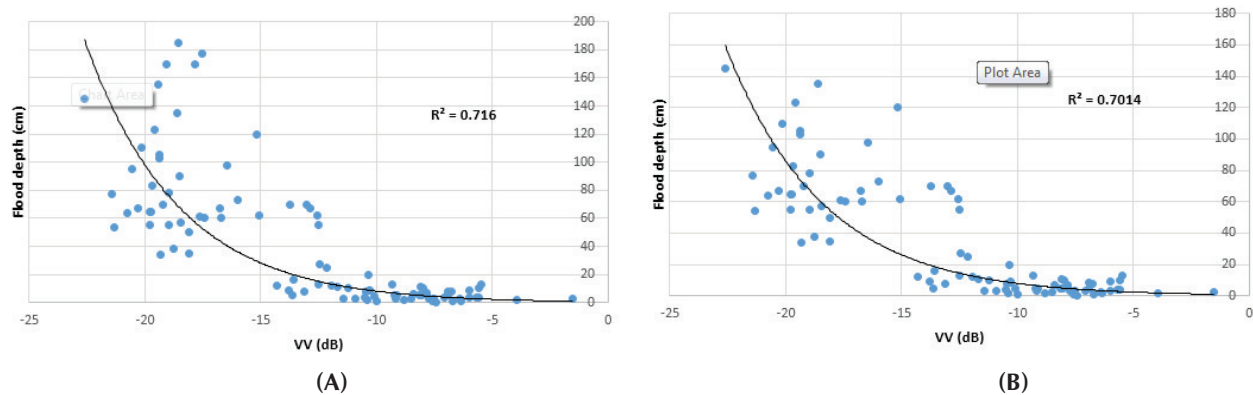


Fig. 6. Correlation between field flood depth and the backscattering value on VV polarization in 2019: (A) correlation coefficient (96 samples), (B) correlation coefficient (91 eliminated samples).

Flood depth threshold in 2019 in An Giang province

The VV polarization results were used to create thresholds and develop flood depth maps (Table 5). It was shown that there was not much difference between the imagery values (dB) thresholded as a water object during the three months of flooding because the flooding levels were different, thus the backscattering values were not the same. In general, a low backscattering value indicates the presence of water and, in contrast, a high backscattering value does not indicate the presence of water.

Table 5. Correlation between backscattering values and water values on Sentinel 1A images during three months in 2019.

No.	Date	Imagery values (dB)	Water values (dB)
1	06/08/2019	+30,6 to -24,8	-12 to -24,8
2	11/09/2019	+22,4 to -26,2	-14 to -26,2
3	05/10/2019	+14,7 to -25,4	-16 to -25,4

Discussion

This research aimed to detect flood depth using Sentinel-1 data for recording water levels changes from August to October 2019 in the An Giang province, which is an upstream province in the Mekong river delta. Sentinel-1 SAR imagery proved an effective tool for excellent spatiotemporal dynamic of flood depth maps and offers the possibility of processing an entire study area based on the extent of spatial coverage for each image. Mapping development for the variations in water depth levels in the study area before, during, and after the flood event was also feasible with Sentinel-1 imagery. The flood season occurred from May to November in 2019 with the flood extent taking place in October 2019 outside the dyke when floods covered nearly the entire the An Giang province. It was also proved that there was a high correlation between backscatter value and flood depth value during the flood event and limited backscatter values for flood depths on Sentinel 1A images.

Flood depth maps created from Sentinel-1 SAR images complement and validate information that elucidates the spatial and temporal evolution of floods. The results advise the use of Sentinel-1 SAR images to derive flood depth by the calibration and evaluation of hydrological models and as a data source that can be analysed using other methodologies.

Sentinel 1A data was collected from August to October 2019 and, in this research, could not show a series map of flooded areas during rainy season periods. Also, the impact of a drainage system was not mentioned in this research to analyse water withdrawal in an inundated area.

The research must take into consideration that satellite observations allow one to outline a flooded area and estimate the water depth at the specific date and time during the flood events corresponding to a minimum and maximum water depth classification. Future work may consider integrating a DEM filling procedure for water level estimation to indicate an error in the flood map and its corresponding elevation. This would be information that improves the statistics and estimation of the water levels.

Conclusions

This study has determined a correlation between the values of field flood depth and backscattering values from Sentinel-1A image polarizations with high correlation coefficients ($r > 0.8$ (0.84-0.98) and the coefficients of determination $R^2 > 0.75$ (0.79-0.95) for three months (August, September and October) in 2019. At the same time, flood depths were observed to range from 0-250 cm with five water depth levels. In August, the area was the lowest with 21,601.65 ha (accounting for 6.31%) of the total provincial flooded area and was divided into two levels of flood depths ranging from 0-50 cm. In September the flooded area increased to 56,656.75 ha (accounting for 16.54%) and was divided into three levels of flood depth corresponding to depths ranging from 0-100 cm. In October the distribution of flood depth reached its peak with the highest flooded area of 89,606.82 ha (accounting for 26.15%) and was divided into four levels of flooding corresponding to the depth of flood from 10-250 cm. This study determined the threshold of flood depth using Sentinel-1A images below 145 cm. If the depth of flood exceeds this value, the scattering value on the image will not find a difference in the field flood depth.

ACKNOWLEDGEMENTS

The authors thank the Department of Science and Technology in the An Giang province, which has been very helpful in providing valuable materials and supporting us during the survey. We highly appreciate the valuable funding in part by the Technological

Cooperation Project “Building capacity for Can Tho University to be an excellent institution of education, scientific research and technology transfer” of JICA. Our gratitude extends to the Can Tho University Improvement Project VN15-P6 which was funded by a Japanese ODA loan to all those who provided us the possibility to complete this research in ODA-E3 project. Lastly, but of equal importance, we owe a great debt to the project management board and colleagues at the College of Environment and Natural Resources to support us during the accomplishment of this project. We thank the European Space Agency for providing us with the satellite data used in this study.

COMPETING INTERESTS

The authors declare that there is no conflict of interest regarding the publication of this article.

REFERENCES

- [1] Ministry of Agriculture and Rural Development (MARD) (2010), *Flood Proofing for Poor Coastal and Inland Households in the Mekong River Delta in Viet Nam - Pilot in An Giang Province*, United Nations Development Program, Project Duration: 11/1-30/9/2007, Program Component: Environment and Energy for Sustainable Development.
- [2] F. Frappart, et al. (2006), “Water volume change in the lower Mekong from satellite altimetry and imagery data”, *Geophysical Journal International*, **167**, pp.570-584.
- [3] S.J. Birkinshaw, et al. (2010), “Using satellite altimetry data to augment flow estimation techniques on the Mekong river”, *Hydrological Processes*, **24**, pp.3811-3825.
- [4] A.A. Jarihani, et al. (2013), “Evaluation of multiple satellite altimetry data for studying inland water bodies and river floods”, *Journal of Hydrology*, **505**, pp.78-90.
- [5] F. Baup, F. Frappart, J. Maubant (2014), “Combining high-resolution satellite images and altimetry to estimate the volume of small lakes”, *Hydrology and Earth System Sciences*, **18**, DOI: 10.5194/hess-18-2007-2014.
- [6] M.M. Islam, and K. Sado (2000), “Development of flood hazard maps of Bangladesh using NOAA-AVHRR images with GIS”, *Hydrological Sciences Journal*, **45**(3), pp.337-355.
- [7] D. Raclot (2006), “Remote sensing of water levels on floodplains: a spatial approach guided by hydraulic functioning”, *International Journal of Remote Sensing*, **27**, pp.2553-2574.
- [8] R. Hostache, X. Lai, J. Monnier, C. Puech (2010), “Assimilation of spatially distributed water levels into a shallow-water flood model. Part II: use of a remote sensing image of Mosel river”, *Journal of Hydrology*, **390**, pp.257-268.
- [9] P. Matgen, et al. (2007), “Integration of SAR-derived river inundation areas, high-precision topographic data and a river flow model toward near real-time flood management”, *International Journal of Applied Earth Observation and Geoinformation*, **9**(3), pp.247-263.
- [10] G. Schumann, et al. (2007), “High-resolution 3-D flood information from radar imagery for flood hazard management”, *IEEE Transactions on Geoscience and Remote Sensing*, **45**, pp.1715-1725.
- [11] D.C. Mason, et al. (2007), “Improving river flood extent delineation from synthetic aperture radar using airborne laser altimetry”, *IEEE Transactions on Geoscience and Remote Sensing*, **45**(12), pp.3932-3943.
- [12] F. Pan, et al. (2013), “Application of the inundation area - lake level rating curves constructed from the SRTM DEM to retrieving lake levels from satellite measured inundation areas”, *Computers & Geosciences*, **52**, pp.168-176.
- [13] D.C. Mason, et al. (2016), “Improving the tan DEM-X digital elevation model for flood modeling using flood extents from synthetic aperture radar images”, *Remote Sensing of Environment*, **173**, pp.15-28.
- [14] K. Chen, R.M. Horton, D.A. Bader, C. Lesk, L. Jiang, B. Jones, L. Zhou, X. Chen, J. Bi, P.L. Kinney (2017), “Impact of climate change on heat-related mortality in Jiangsu province, China”, *Environ. Pollut.*, **224**, DOI: 10.1016/j.envpol.2017.02.011.
- [15] Z.N. Musa, I. Popescu, A. Mynett (2015), “A review of applications of satellite SAR, optical, altimetry and DEM data for surface water modeling, mapping and parameter estimation”, *Hydrology and Earth System Sciences*, **19**, pp.3755-3769.
- [16] S. Grimaldi, et al. (2016), “Remote sensing-derived water extent and level to constrain hydraulic flood forecasting models: opportunities and challenges”, *Surveys in Geophysics*, **37**, pp.977-1034.
- [17] G.J.P. Schumann, A. Domeneghetti (2016), “Exploiting the proliferation of current and future satellite observations of rivers”, *Hydrol. Process.*, **30**, pp.2891-2896.
- [18] G.J.P. Schumann, D.K. Moller (2015), “Microwave remote sensing of flood inundation”, *Phys. Chem. Earth Parts A/B/C*, pp.84-95.
- [19] P.D. Bates, M.S. Horritt, C.N. Smith, D.C. Mason (1997), “Integrating remote sensing observations of flood hydrology and hydraulic modelling”, *Hydrol. Process.*, **11**, pp.1777-1795.
- [20] G. Aronica, P.D. Bates, M.S. Horritt (2002), “Assessing the uncertainty in distributed model predictions using observed binary pattern information within GLUE”, *Hydrol. Process.*, **16**, pp.2001-2016.
- [21] J. Garcia-Pintado, J.C. Neal, D.C. Mason, S.L. Dance, P.D. Bates (2013), “Scheduling satellite-based SAR acquisition for sequential assimilation of water level observations into flood modelling”, *Journal of Hydrology*, **495**, pp.252-266.
- [22] P. Matgen, M. Montanari, R. Hostache, L. Pfister, L. Hoffmann, D. Plaza, et al. (2010), “Towards the sequential assimilation of SAR-derived water stages into hydraulic models using the particle filter: proof of concept”, *Hydrology and Earth System Sciences*, **14**(9), pp.1773-1785.
- [23] P.D. Bates (2012), “Invited commentary: integrating remote sensing data with flood inundation models: how far have we got?”, *Hydrol. Process.*, **26**, pp.2515-2521.
- [24] G.J.P. Schumann, P.D. Bates, M.S. Horritt, P. Matgen, F. Pappenberger (2009), “Progress in integration of remote sensing derived flood extent and stage data and hydraulic models”, *Rev. Geophys.*, **47**, DOI: 10.1029/2008RG000274.
- [25] G. Di Baldassarre, G. Schumann, P.D. Bates (2009), “A technique for the calibration of hydraulic models using uncertain satellite observations of flood extent”, *Journal of Hydrology*, **367**, pp.276-282.
- [26] M.S. Horritt and P.D. Bates (2002), “Evaluation of 1-D and 2-D numerical models for predicting river flood inundation”, *Journal of Hydrology*, **268**, pp.87-99.
- [27] P.D. Bates, M.S. Horritt, G. Aronica, et al. (2004), “Bayesian updating of flood inundation likelihoods conditioned on flood extent data”, *Hydrol. Process.*, **18**, pp.3347-3370.
- [28] https://en.wikipedia.org/wiki/An_Giang_Province (accessed on 10 May 2020).
- [29] Benedikter (2013), *The Vietnamese Hydrocracy and the Mekong Delta*, ISBN 9793643904379.
- [30] V.H.T. Duong, T. Van, F. Nestmann, P. Oberle, N.T. Nam (2014), *Land Use Based Flood Hazards Analysis for Mekong Delta*, Proceedings 19th IAHR Asian and Pacific Regional Division 2014, DOI: 10.13140/2.1.5153.9842
- [31] F. De Zan, A. Monti Guarnieri (2006), "Terrain Observation by Progressive Scans, September", *IEEE Transactions on Geoscience and Remote Sensing*, **44**(9), pp.2352-2360.
- [32] <https://sentinel.esa.int/web/sentinel> (accessed on 8 August 2019).
- [33] <https://step.esa.int/main/download/snap-download> (accessed on 22 December 2019).
- [34] B. Tavus, S. Kocaman, C. Gokceoglu, H.A. Nefeslioglu (2018), “Considerations on the use of Sentinel-1 data in flood mapping in urban areas: Ankara (Turkey) 2018 floods”, *Int. Arch. Photogram. Remote Sens. Spat. Inf. Sci.*, **XLII-5**, pp.575-581.
- [35] H.-J. Ban, Y.-J. Kwon, H. Shin, H.-S. Ryu, S. Hong (2017), “Flood monitoring using satellite-based RGB composite imagery and refractive index retrieval in visible and near-infrared bands”, *Remote Sens.*, **9**, DOI: 10.3390/rs9040313.
- [36] J.-M. Park, W.J. Song, W.A. Pearlman (1999), “Speckle filtering of SAR images based on adaptive windowing”, *IEE Proc. Vis. Image Signal Proces.*, **146**, pp.191-197.
- [37] E. Nazry, A. Lopes, R. Touzi (1991), *Detection of Structural and Textural Features for SAR Images Filtering*, Proceedings of IGARSS, **91**, pp.2169-2172.
- [38] A. Lopes, E. Nezry, R. Touzi, H. Laur (1993), “Structure detection and statistical adaptive speckle filtering in SAR images”, *Int. J. Remote Sens.*, **14**(9), pp.1735-1758.
- [39] L. Pulvirenti, M. Chini, N. Pierdicca, L. Guerriero, P. Ferrazzoli (2011), “Flood monitoring using multitemporal COSMO-SkyMed data: image segmentation and signature interpretation”, *Remote Sens. Environ.*, **115**(4), pp.990-1002.